Synthesis and Characterization of Mesoporous Chromium-Containing Silica Tube Molecular Sieves CrMCM-41

Zhidong Zhu, Zhixiang Chang, and Larry Kevan*

Department of Chemistry, University of Houston, Houston, Texas 77204-5641

Received: December 17, 1998; In Final Form: February 10, 1999

A series of mesoporous chromium-containing silica tube molecular sieves (CrMCM-41) with variable Si/Cr ratios have been synthesized and characterized by powder X-ray diffraction (XRD), electron probe microanalysis (EPMA), Fourier transform infrared spectroscopy (FTIR), diffuse reflectance UV−visible spectroscopy (UV−vis), electron spin resonance (ESR), electron spin-echo modulation (ESEM), Raman spectroscopy, ^{29}Si magic-angle-spinning nuclear magnetic resonance (MAS NMR), and N_2 adsorption measurements. XRD, EPMA, UV−vis, and ESR show that the as-synthesized CrMCM-41 materials have the MCM-41 structure and contain only atomically dispersed Cr(III). FTIR, UV−vis, and Raman reveal that Cr(VI) monochromate exists in calcined CrMCM-41. ^{29}Si MAS NMR and N_2 adsorption show that part of the chromium is incorporated into the MCM-41 structure. ESR shows that Cr(VI)−O_2^- exists in calcined CrMCM-41 and transforms to Cr(V) after evacuation above 150 °C. The interaction of Cr(V) with O_2, CO, C_2D_4, ND_3, CD_3OH, and D_2O was studied. Cr(V) occurs at two different sites. At one site, Cr(V) coordinates with one molecule of O_2, CO, and D_2O to form square pyramidal complexes and reacts with C_2D_4, CD_3OH, and ND_3 to be reduced to Cr(III). At the other site, Cr(V) is inert to O_2, CO, and C_2D_4 while it coordinates with two molecules of ND_3 to form six-coordinated complexes and coordinates with one molecule of CD_3OH.

Introduction

Chromium compounds have been widely used as catalysts for selective oxidation of various organic substrates.[1,2] Chromium-containing molecular sieves have attracted catalytic interest.[3−6] Several chromium-containing molecular sieves such as CrS-1,[7,8] Cr-β,[9] CrAPSO-5,[6,10,11] CrAPSO-11,[12,13] and CrAPSO-34[14] have been synthesized and characterized. However, these molecular sieves are microporous solids with channels less than 10 Å which are too small for the oxidation of large organic molecules.

Supported chromium oxide catalysts are crucial for the production of several important commodity chemicals in the chemical industry. Cr/SiO_2 catalysts are known as Philips catalysts and are used for the production of high-density and linear low-density polyethylene.[15] Cr/Al_2O_3 catalysts are industrially used for the production of isobutene and propene.[16]

The hexagonal tubular silica materials, MCM-41, possess uniform mesopore channels varying from about 15 to 300 Å,[17−20] which allow faster diffusion of large organic molecules than smaller channel microporous molecular sieves. The uniformity of the mesopore makes MCM-41 a better support than amorphous silica. This opens an opportunity for the preparation of chromium-containing mesoporous molecular sieve materials. There are two recent communications about Cr-containing mesoporous materials.[21,22] But the exact nature of chromium in mesoporous molecular sieves needs further elucidation. The elucidation of the distribution, oxidation state, and coordination of these Cr species on MCM-41 is of fundamental importance for understanding the catalytic role of Cr in CrMCM-41.

Characterization of the local environment of the chromium in CrMCM-41 requires a combination of spectroscopic techniques because chromium can change its oxidation state and coordination geometry on thermal and other treatments used in catalytic applications. In this work a systematic study of CrMCM-41 by powder X-ray diffraction (XRD), electron probe microanalysis (EPMA), Fourier transform infrared (FTIR), diffuse reflectance UV−visible spectroscopy (UV−vis), electron spin resonance (ESR), electron spin-echo modulation (ESEM), Raman spectroscopy, ^{29}Si MAS NMR, and N_2 adsorption is given. The results show that chromium is highly dispersed in CrMCM-41 and that various chromium species in different oxidation states and with different coordinations occur in MCM-41.

Experimental Section

Synthesis. Fumed silica was used as the silicon source, and chromium chloride hexahydrate ($CrCl_3 \cdot 6H_2O$) was used as the chromium source. CrMCM-41 was synthesized following a modified method for purely siliceous MCM-41. A typical synthesis procedure is as follows. A 10 g 35% solution of tetraethylammonium hydroxide (TEAOH) is combined with 6.2 g of cetyltrimethylammonium bromide (CTAB) dispersed in 49 g of water with stirring and heating at 50 °C for 0.5 h; then 6 g of silica is added and stirred for 2 h. At the same time, an amount of chromium chloride hexahydrate for the desired Si/Cr ratio is dissolved in 5 g of water and then slowly added to the silica gel with stirring. The pH of the mixture is adjusted to 11.5 by addition of dilute sulfuric acid. Finally, the gel mixture is transferred into an autoclave and heated at 150 °C for 2 days. The molar composition of the final gel mixture was 1.0 SiO_2:0.17 CTAB:x Cr_2O_3:0.24 TEAOH:30 H_2O with x = 0−0.0125. The solid products were recovered by filtration, washed with deionized water, and dried in air. These samples are designated as CrMCM-41-(x), where x is the Si/Cr ratio in the gel, or MCM-41 for purely siliceous MCM-41. All the as-synthesized samples are calcined by raising the temperature slowly to 823 K in flowing N_2 and then keeping the sample at

10.1021/jp984771p CCC: $18.00
Published on Web 03/18/1999

this temperature for 15 h in flowing air for removal of CTAB. The calcined samples are cooled under N_2 and kept in a desiccator. The calcined samples are dried overnight at 150 °C before all measurements. So the calcined samples are dehydrated.

Measurements. The elemental composition of the resultant solid products was analyzed by EPMA using a JEOL JXA-8600 spectrometer.

Powder XRD patterns of the calcined products were obtained on a Philips 1840 diffractometer with Cu Kα radiation (40 kV, 25 mA) at a 0.01 step size and 1 s step time over the range $1.2° < 2\theta < 10°$. The samples were prepared as thin layers on aluminum slides.

Diffuse reflectance UV−vis spectra were measured with a Perkin-Elmer 330 spectrophotometer equipped with a 60 mm Hitachi integrating sphere accessory. Powder samples were loaded into an evacuable quartz cell with Suprasil windows, and spectra were collected in the 200−800 nm wavelength range against a MCM-41 standard.

FTIR measurements were performed on a Nicolet 740 FTIR spectrophotometer using the KBr self-supported pellet technique. The pellets contained about 1% of finely powdered sample and were pressed at 4 ton/cm^2.

The Raman spectra were acquired on a 1 cm diameter round solid pellet of the samples (no KBr) at room temperature. The laser line used was 458 nm from a Coherent K-2 continuous wave (cw) krypton ion laser to minimize the fluorescence background. The laser power at the samples was 250 mW. The sample was rotated at about 1000 rpm in the laser beam to minimize sample heating. A lower laser power of 100 mW gave the same spectrum with increased noise. The Raman data were obtained at 1 cm^{-1} increments over 450−1100 cm^{-1} and three scans were averaged.

MAS NMR spectra were obtained with a Unity-400 Varian NMR spectrometer and a Doty high-speed probe. The ^{29}Si resonance frequency was 79.47 MHz. Samples were loaded into 5 mm zirconia rotors with Vespel end caps and spun at the magic angle at about 9 kHz. These rotors have an inherent zirconium silicate impurity signal that occurs at −22 ppm with reference to TMS at 0.0 ppm. This can be conveniently used as an internal reference for the chemical shifts and has been double checked with zeolite 4 Å, which exibits a single relatively sharp resonance at −89.6 ppm. A recycle delay of 20 s was used between pulses, the tip angle being 45°. Typically, signal averaging was done overnight to get a decent signal/noise ratio.

X-band ESR spectra were recorded in sealed Suprasil quartz tubes at 77 K with a Bruker ESP 300 ESR spectrometer. ESEM spectra were recorded at 5 K with a Bruker ESP 380 pulsed FT-ESR spectrometer. Three-pulse echoes were recorded with a $\pi/2-\tau-\pi/2-T-\pi/2$ pulse sequence as a function of T. The value of τ in the three-pulse experiment was optimized to enhance the modulation of deuterium. Echo modulation patterns were simulated using a point-dipole spherical averaging approximation. The number of interacting nuclei N at distance R with isotropic hyperfine coupling A_{iso} were determined by fitting simulations to experimental data.[23,24]

N_2 adsorption isotherms were measured at 77 K using a Micromeritics Gemini 2375 analyzer. Prior to adsorption, samples were dehydrated at 300 °C for 5 h. The specific surface area, A_{BET}, was determined from the linear part of a BET plot ($p/p_0 = 0.05-0.30$). The pore size distribution was calculated using the adsorption branches of the N_2 adsorption isotherm and the Barrett−Joyner−Halenda (BJH) formula.[25] The cumulative mesopore surface area, A_{BJH}, was obtained from the pore size distribution.

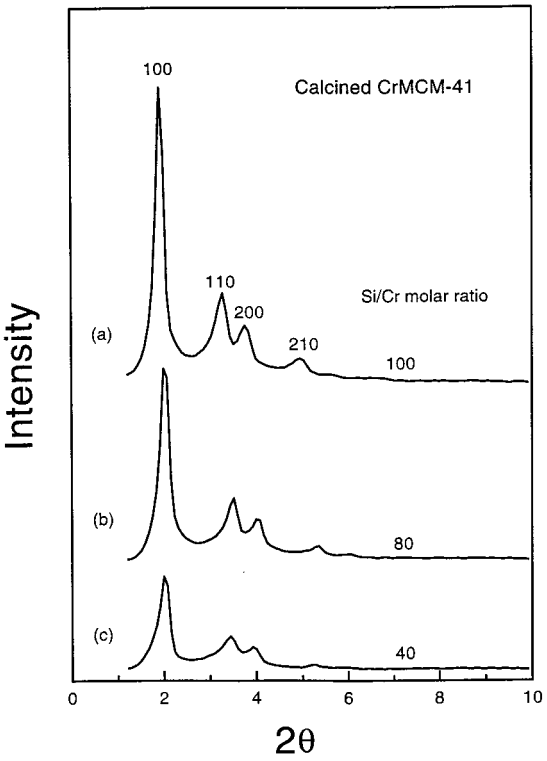

Figure 1. XRD patterns of calcined, dehydrated CrMCM-41: (a) CrMCM-41-(100), (b) CrMCM-41-(80), and (c) CrMCM-41-(40).

Results

Synthesis and Elemental Analysis. In most of the reported syntheses of pure siliceous MCM-41 materials and their metal derivatives, NaOH was introduced in the synthesis gel. It is known, however, that there is a detrimental effect of alkali metal ions on the catalytic properties of transition metal-containing silicate molecular sieves.[26] So we chose silica as the silicon source and TEAOH as the hydroxide source. A higher synthesis temperature corresponds to a larger unit cell with thicker and more highly polymerized walls.[27] So samples prepared at high temperatures have the smaller contraction of the unit cell upon calcination. So we chose 150 °C as the synthesis temperature rather than 100 °C. But at 150 °C the hexagonal phase is easily transformed into a lamellar or amorphous phase after 2 days. So we limited the crystallization time to 2 days.

EMPA shows that chromium is homogeneously distributed throughout the CrMCM-41 solid particles. The chromium compositions of the solid products as determined by EMPA are in good agreement with the gel compositions.

XRD. The well-defined pattern in Figure 1 is typical of MCM-41 as described by Kresge et al.[17,18] All four XRD reflections (100), (110), (200), and (210) are resolved and can be indexed to a hexagonal lattice. The (110), (200), and (210) reflections were not resolved for CrMCM-41 prepared earlier.[21] Upon calcination of the as-synthesized product, the intensity of the XRD peaks increases by a factor of more than 2 and there is no framework contraction (not shown). This indicates that our material is highly polymerized and ordered. It was reported that the unit cell parameter increases with increasing Cr content.[21] However, we observe the opposite. The d_{100} spacing slightly decreases with increasing Cr content, which is similar to GaMCM-41.[28] The intensity of the (100) peak

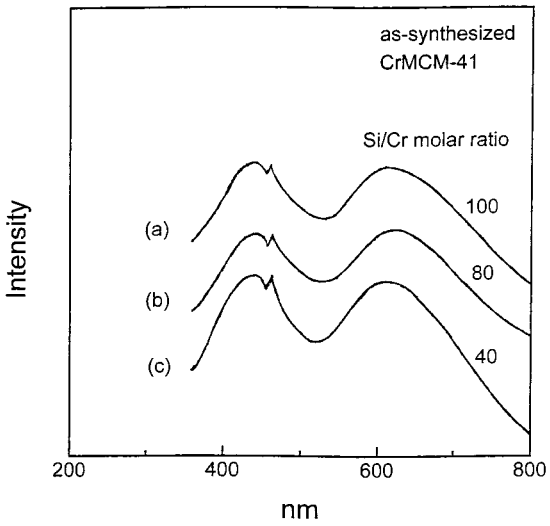

Figure 2. Diffuse reflectance UV−vis spectra of as-synthesized CrMCM-41 with various Si/Cr ratios: (a) CrMCM-41-(100), (b) CrMCM-41-(80), and (c) CrMCM-41-(40).

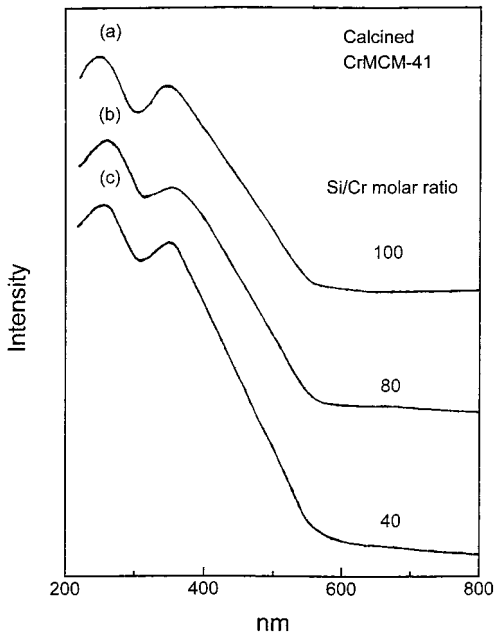

Figure 3. Diffuse reflectance UV−vis spectra of calcined, dehydrated CrMCM-41 with various Si/Cr ratios: (a) CrMCM-41-(100), (b) CrMCM-41-(80), and (c) CrMCM-41-(40).

decreases with increasing Cr content. This may be due to partial structural collapse upon calcination, associated with the formation of macropores upon calcination, as observed by N_2 adsorption (see below).

UV−Vis. Figures 2 and 3 show UV−vis spectra of as-synthesized and calcined, dehydrated CrMCM-41, respectively. The spectra of as-synthesized CrMCM-41 contains two typical bands of octahedral Cr(III) at 445 and 611 nm. They have been assigned to d−d transitions described as $^4A_{2g} \rightarrow {}^4T_{2g}$ and $^4A_{2g} \rightarrow {}^4T_{1g}$ transitions, respectively.[1] The sharp shoulder at 467 nm in Figure 2 can be assigned to a spin forbidden $^4A_{2g} \rightarrow {}^2T_{2g}$ transition of six-coordinate Cr(III) under tetragonal distortion.[29]

The spectra of calcined, dehydrated CrMCM-41 are dominated by two intense bands around 259 and 350 nm. These bands are usually assigned as O → Cr (VI) charge transfers of a chromate species.[1] A band around 440 nm characteristic of Cr(VI) polychromate is not observed.[1] These results indicate

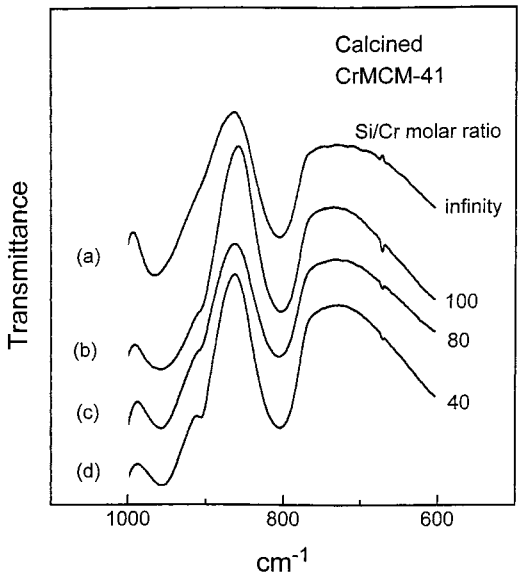

Figure 4. FTIR absorption spectra of (a) calcined, dehydrated siliceous MCM-41, (b) calcined, dehydrated CrMCM-41-(100), (c) calcined, dehydrated CrMCM-41-(80), and (d) calcined, dehydrated CrMCM-41-(40).

that Cr(VI) monochromate (CrO_4^{2-}) and not higher chromates exist in calcined CrMCM-41, which is consistent with the Raman results (see below).

In both Figures 2 and 3 it is observed that the intensities of these transitions do not increase linearly with loading over the full range investigated. As the Cr loading increases, the penetration depth of the light beam decreases so that fewer particles are probed. Also, the relative fraction of specularly reflected light increases.

FTIR. The IR spectra of calcined, dehydrated MCM-41 and CrMCM-41 are shown in Figure 4. Although these spectra are obtained with the sample pellet in ambient air, rehydration during the sample measurement time of about 30 min or less is considered unlikely because of slow diffusion of air into the solid pellet. The optical density of the band at 905 cm^{-1}, which is absent in calcined MCM-41 increases with the Cr content. It is assigned to a Cr═O or Cr—O vibration from a Cr(VI) species in a dehydrated sample.[30] In all samples a FTIR band around 960 cm^{-1} is observed, which is often assigned to a lattice defect and is correlated with the presence of chromium ions (or other framework ions) in a chromium silicate-1 framework (CrS-1).[7] This 960 cm^{-1} band is also prominent in the FTIR spectrum of calcined siliceous MCM-41. By carefully examining this band, it is at 967 cm^{-1} in siliceous MCM-41 and is shifted to 956 cm^{-1} in CrMCM-41, as shown in Figure 4. Recent work suggests that this band is assignable to a Si−O vibration in a Si—OH group in siliceous MCM-41.[31] If this is the case, it is reasonable to attribute the red shift in CrMCM-41 to the replacement of a OH group by O—Cr(VI). Another band at 680 cm^{-1} is ascribed to an asymmetric vibration of (Si—O—Cr) groups in Cr-ZSM-5 and CrS-1.[32,33] Our results seem to be inconsistent with this observation because the optical density does not proportionally increase with the Cr content. In VMCM-41, the band associated with an asymmetric stretching frequency of framework Si—O—Si bonds shifts from 1089 cm^{-1} (calcined siliceous MCM-41) to 1079 cm^{-1} (calcined VMCM-41).[34] In CrMCM-41 no such shift is observed.

Raman. Figure 5 shows Raman spectra of calcined, dehydrated siliceous MCM-41 and CrMCM-41 (Si/Cr = 40). Although these spectra are obtained with the sample pellet in

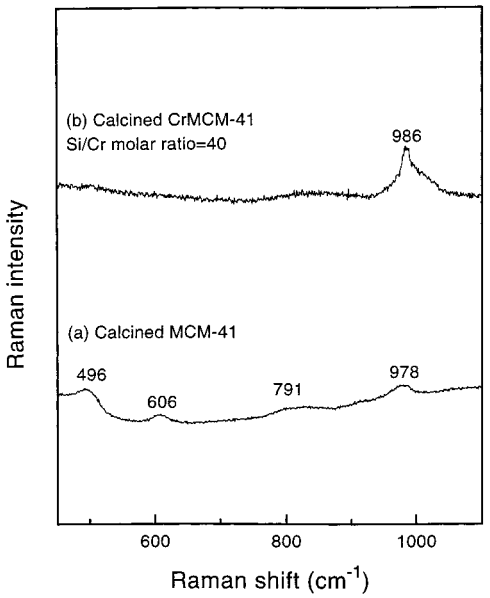

Figure 5. Raman spectra at 293 K of (a) calcined, dehydrated siliceous MCM-41 and (b) calcined, dehydrated CrMCM-41-(40).

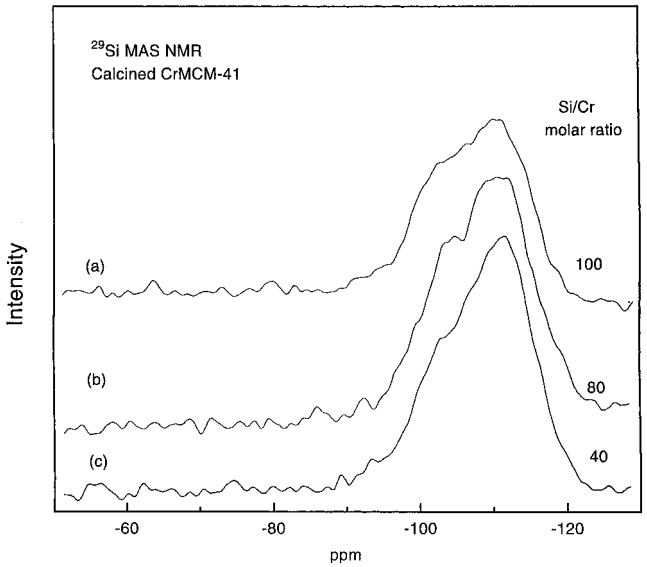

Figure 6. ^{29}Si MAS NMR spectra of calcined, dehydrated CrMCM-41 with various Si/Cr ratios: (a) CrMCM-41-(100), (b) CrMCM-41-(80), and (c) CrMCM-41-(40).

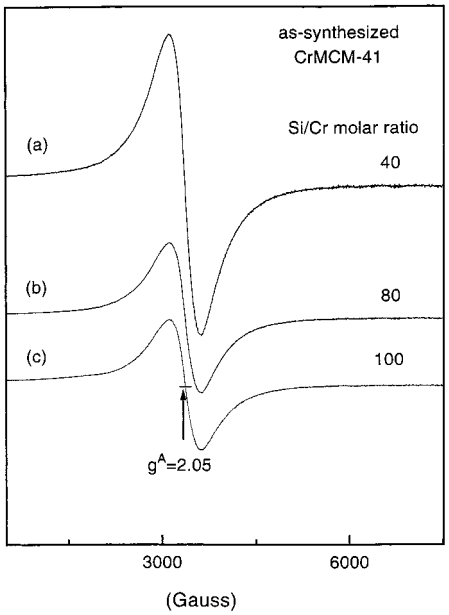

Figure 7. ESR spectra at 77 K of as-synthesized CrMCM-41 with various Si/Cr ratios: (a) CrMCM-41-(40), (b) CrMCM-41-(80), and (c) CrMCM-41-(100).

ambient air, rehydration during the sample measurement time of about 30 min or less is considered unlikely because of slow diffusion of air into the solid pellet. In siliceous MCM-41, the band at 791 cm^{-1} is assigned to siloxane linkages (Si−O−Si), the bands at 496 and 606 cm^{-1} to three Si and four Si siloxane rings and the band at 978 cm^{-1} to surface silanol groups.[35] In contrast, CrMCM-41 gives only a band at 986 cm^{-1}. This is interpreted as follows.

Chromium(VI) oxide compounds prefer tetrahedral coordination for Cr(VI), and various types of tetrahedrally coordinated chromium oxide compounds are known. Tetrahedral coordinated chromium can be monochromate (CrO_4^{2-}), dichromate ($Cr_2O_7^{2-}$), trichromate ($Cr_3O_{10}^{2-}$), or tetrachromate ($Cr_4O_{13}^{2-}$) both in aqueous solution and in a crystalline lattice.[36] In heterogeneous catalysts, Cr(VI) ions are typically anchored as chromate, dichromate, or polychromate species. The characteristic Raman bands of these chromium (VI) oxide species are summarized in Table 2 of ref 1. The Raman band near 986 cm^{-1} in calcined, dehydrated CrMCM-41 is characteristic of a dehydrated monochromate species.[1] It is similar to the Raman spectrum of dehydrated, silica-supported chromium oxide catalysts.[37]

^{29}Si MAS NMR. Figure 6 shows the ^{29}Si MAS NMR of calcined CrMCM-41. The resonance at −101 ppm is attributed to silicon atoms with three siloxane bonds and one silanol group, **Si**$(OSi)_3OH$ (Q^3), while the resonance at −110 ppm is ascribed to silicon atoms with four siloxane bonds, **Si**$(OSi)_4$ (Q^4).[38] Deconvolution of the spectra into two peaks shows that the $f_s = Q^3/(Q^3 + Q^4)$ ratio that characterizes the fraction of silanol groups in calcined CrMCM-41 first increases from 28% to 34% and then decreases to 26% from CrMCM-41-(100) to CrMCM-41-(80) to CrMCM-41-(40). These changes are significantly greater than the measurement error.

In CrS-1 and Cr-ZSM-5, a shoulder around −115 ppm, absent from the spectrum of pure silicate-1 and ZSM-5, is attributed to Si surrounded by three Si and one Cr, confirming the presence of framework Cr ions in the zeolitic structure.[7,33] A weak shoulder at −115 ppm in CrMCM-41 thus supports framework incorporation of Cr. Also a slight Q^4 peak broadening is observed, which may be evidence that isomorphous transition metal substitution has occurred.[22] The slightly increased line width of the ^{29}Si lines from Ti-MCM-41 has been explained in terms of changes in the distribution of Si—O—Si angles in SiO_4 tetrahedra after the incorporation of titanium.[39]

ESR of As-Synthesized and Calcined CrMCM-41. ESR spectra of Cr(III) at $g^A = 2.05$ in as-synthesized CrMCM-41 are shown in Figure 7. No other Cr(III) signals are present in the ESR spectra of the as-synthesized materials. The ESR intensity of Cr(III) increases, while the line width does not increase with Cr content. This indicates that Cr(III) is highly dispersed in as-synthesized CrMCM-41 over the Cr concentration range studied. After calcination, the Cr(III) signal disappears while O_2^- with $g_1^B = 2.05$, $g_2^B = 2.04$, and $g_3^B = 2.03$ appears (Figure 8). The intensity of O_2^- increases linearly with Cr content. The O_2^- signal is not observed in calcined siliceous MCM-41. The g_3^B value of the O_2^- radical is strongly dependent on the positive charge of the nearest cation.[40] Generally, with an increase of the metal ion oxidation state from 1 to 6, g_3 decreases from about 2.15 to about 2.02. The fact that the

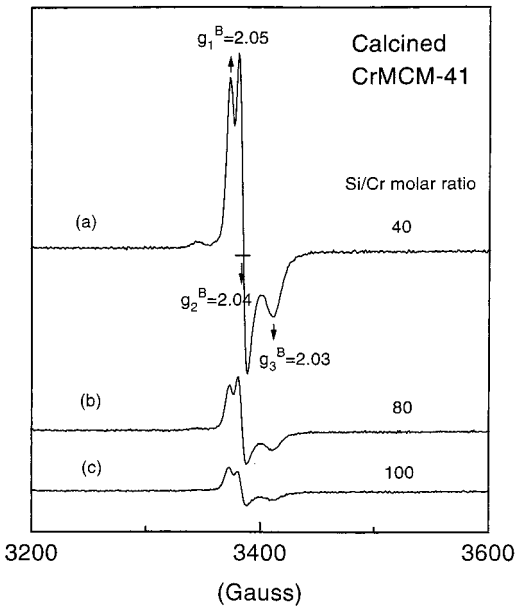

Figure 8. ESR spectra at 77 K of calcined, dehydrated CrMCM-41 with various Si/Cr ratios: (a) CrMCM-41-(40), (b) CrMCM-41-(80), and (c) CrMCM-41-(100).

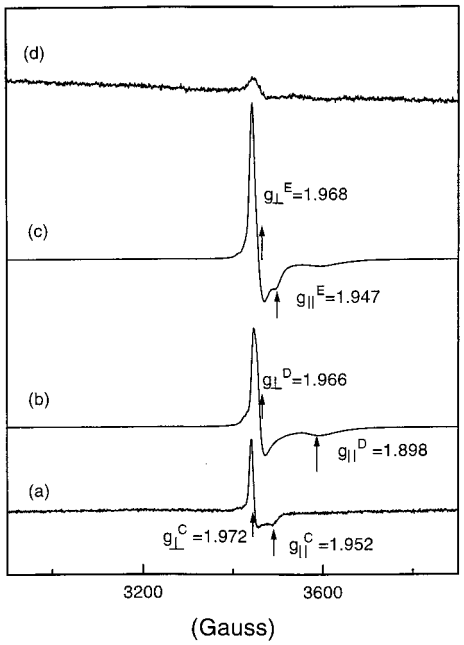

Figure 9. ESR spectra of calcined, dehydrated CrMCM-41: (a) evacuated at room-temperature overnight, (b) evacuated at 150 °C overnight, (c) evacuated at 350 °C overnight followed by oxygen adsorption, and (d) heated at 300 °C for 2 h.

intensity of O_2^- increases linearly with Cr content and that g_3^B is around 2.03 indicates that O_2^- is connected with Cr(VI) to form Cr(VI)−O_2^-.

After calcined CrMCM-41 is evacuated at room temperature overnight, a weak signal of Cr(V) with $g_\perp^C = 1.972$ and $g_\parallel^C = 1.952$ is observed and assigned to square-pyramidal Cr(V)−O_2[11,13] (Figure 9). After CrMCM-41 is evacuated above 150 °C overnight, Cr(V) with $g_\perp^D = 1.966$ and $g_\parallel^D = 1.898$ is observed and assigned to tetrahedral Cr(V).[11,13] With an increase of the evacuation temperature, the intensity of species D increases. Thus Cr(VI) is reduced to Cr(V) during evacuation above 150 °C, which is defined as "activation". After oxygen adsorption, only part of the Cr(V) interacts with O_2 to form a

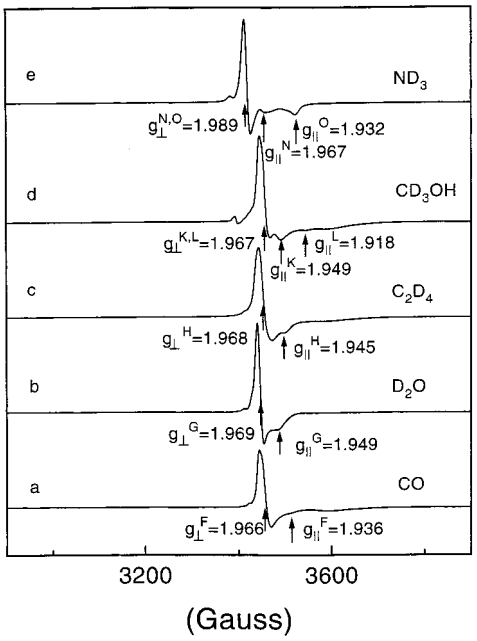

Figure 10. ESR spectra at 77 K of evacuated CrMCM-41 at 350 °C after (a) CO adsorption, (b) D_2O adsorption, (c) C_2D_4 adsorption for 30 min, (d) CD_3OH adsorption for 10 min, and (e) ND_3 adsorption for 10 min.

square pyramidal Cr(V)−O_2 complex with $g_\perp^E = 1.968$ and $g_\parallel^E = 1.947$ similar to species C. This complex is decomposed after evacuation at 60 °C for 2 h. Cr(V) is still observed after oxidation at 300 °C for 2 h using 760 Torr oxygen.

ESR of CrMCM-41 with Adsorbates. ESR spectra for dehydrated, calcined CrMCM-41 after adsorbing CO, D_2O, C_2D_4, CD_3OH, and ND_3 are given in Figure 10. When CO is adsorbed on activated CrMCM-41, a new Cr(V) species with $g_\perp^F = 1.966$ and $g_\parallel^F = 1.936$ is observed. The interaction of CO with Cr(V) is so weak that $g_\parallel$ is very weak (Figure 10a). When D_2O is adsorbed on activated CrMCM-41, a new species with $g_\perp^G = 1.969$ and $g_\parallel^G = 1.949$ is observed (Figure 10b).

When C_2D_4 is adsorbed on activated CrMCM-41 for 0.5 h, a new Cr(V) species with $g_\perp^H = 1.968$ and $g_\parallel^H = 1.945$ is observed. After adsorption of C_2D_4 overnight, a new signal with $g_\perp^I = 4.442$ and $g_\parallel^I = 4.061$ is observed (Figure 11a). After this sample is sealed and kept at room temperature for several days, a broad line at $g^J = 1.994$ is assigned to Cr(III). However, Cr(V) is still observed (Figure 11b).

When CD_3OH is adsorbed on activated CrMCM-41 for 10 min, two new Cr(V) species with $g_\perp^K = 1.967$ and $g_\parallel^K = 1.949$ for species K and $g_\perp^L = 1.967$ and $g_\parallel^L = 1.918$ for L are observed (Figure 10d). After methanol adsorption for 1.5 h, species L disappears and species K remains. There is a weak broad signal around $g^M = 2.00$, which could be Cr(III) from reduction of Cr(V) (not shown). After adsorption of CD_3OH overnight, Cr(V) and Cr(III) disappear due to the further reduction to Cr(II).

When ND_3 is adsorbed on activated CrMCM-41 for 10 min, two new Cr(V) species with axially symmetric ESR parameters ($g_\perp^N = 1.989$ and $g_\parallel^N = 1.967$ for species N and $g_\perp^O = 1.989$ and $g_\parallel^O = 1.932$ for species O) are observed (Figure 10e). After this sample is sealed and kept at room temperature for several days, species O remains and species N disappears. Two new species near $g_\perp^P = 2.430$, $g_\parallel^P = 1.758$, $A_\perp^P = 245$ G and $g_\perp^Q = 4.107$ and $g_\parallel^Q = 1.642$ are observed and assigned to Cr(III)-$(ND_3)_n$ complexes (Figure 11c). The ESR parameters of the various Cr(V) and Cr(III) species are summarized in Table 1.

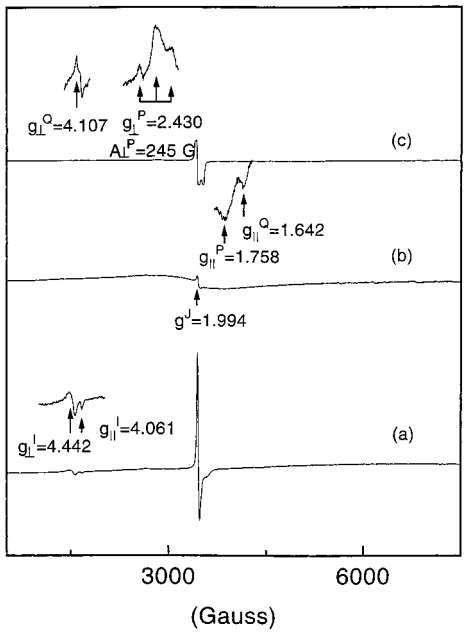

Figure 11. (a) ESR spectra at 77 K of CrMCM-41 evacuated at 350 °C after C_2D_4 adsorption overnight, (b) sample (a) kept at room temperature for several days, and (c) sample (a) after ND_3 adsorption for 10 min and kept at room temperature for several days.

TABLE 1: ESR Parameters of Paramagnetic Cr Species in CrMCM-41 for Various Treatments

$g_\perp$ sample treatment	$g_{||}$ species	g_1	g_2	g_3	g_{iso}
as-synthesized	A: Cr(III)				2.05
calcined	B: Cr(VI)−O_2^-	2.05	2.04	2.03	
evacuated at RT	C: Cr(V)−O_2	1.972	1.952		
evacuated at 150 °C	D: Cr(V)	1.966	1.898		
+O_2	E: Cr(V)−O_2	1.968	1.947		
+CO	F: Cr(V)−CO	1.966	1.936		
+D_2O	G: Cr(V)−D_2O	1.969	1.949		
+C_2D_4	H: Cr(V)−C_2D_4	1.968	1.945		
	I: Cr(IV)	4.442	4.061		
	J: Cr(III)				1.994
+CD_3OH	K: Cr(V)−CD_3OH	1.967	1.949		
	L: Cr(V)−$(CD_3OH)_n$	1.967	1.918		
	M: Cr(III)				2.00
+ND_3	N: Cr(V)−$(ND_3)_n$	1.989	1.967		
	O: Cr(V)−$(ND_3)_2$	1.989	1.932		
	P: Cr(III)−$(ND_3)_n$	2.430	1.758		
	Q: Cr(III)−$(ND_3)_n$	4.107	1.642		

TABLE 2: ^{2}H ESEM Simulation Parameters for Cr(V) in Calcined CrMCM-41 with Various Adsorbates

adsorbate	*N*	*R*, Å	A_{iso}, MHz
D_2O	2	2.9	0.15
CD_3OH	3	3.5	0.10
ND_3	6	3.1	0.04
C_2D_4	4	3.3	0.06

Electron Spin-Echo Modulation. Three-pulse ESEM spectra were recorded at magnetic fields corresponding to $g_\perp$ of various Cr(V) species. ^{2}H ($I = 1$, $\upsilon = 2.288$ MHz, 99.8%) nuclei were investigated for spin-echo modulation. Table 2 summarizes the ESEM parameters. Simulation of the experimental spectrum of CrMCM-41 with adsorbed D_2O gives two deuterium nuclei at 2.9 Å. This is consistent with one D_2O molecule coordinating directly with Cr(V). The spectrum of CrMCM-41 after adsorbing CD_3OH for 1.5 h to form only species K can be simulated by three deuterium nuclei at 3.5 Å. These parameters can be rationalized in terms of one directly interacting methanol. Analysis of the three-pulse ESEM spectra of CrMCM-41 with adsorbed ND_3 to form only species O indicates that Cr(V) is coodinated to two ND_3 molecules at a Cr−D distance of 3.1 Å (Figure 12). The ESEM data for dehydrated CrMCM-41 with adsorbed C_2D_4 indicates that Cr(V) coordinates to one molecule at a Cr−D distance of 3.3 Å.

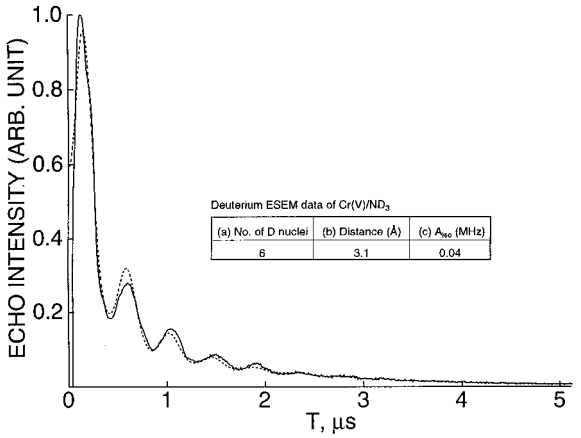

Figure 12. Experimental (—) and simulated (- - -) three-pulse deuterium ESEM spectra at 5 K of CrMCM-41 after ND_3 adsorption for 1.5 h. (a) Number of deuterium nuclei interacting with Cr(V). (b) Distance between deuterium and Cr(V); estimated uncertainty is ±0.1 Å. (c) Isotropic hyperfine coupling constant; estimated uncertainty is ±10%.

N_2 Adsorption Isotherms. Low-temperature nitrogen adsorption isotherms enable the measurement of the surface area, pore volume, and mesopore size distribution. The N_2 adsorption isotherm for calcined CrMCM-41-(100) is a type IV adsorption isotherm typical of mesoporous solids with H2 hysteresis.[41] Adsorption at low pressures ($p/p_0 < 0.35$) is accounted for by monolayer−multilayer adsorption of N_2 on the walls of the mesopores. At a relative pressure p/p_0 between 0.35 and 0.45, the isotherm exhibits a sharp inflection characteristic of capillary condensation within the mesopores. The sharpness in this step indicates a uniform pore size. The amount of the N_2 adsorbed is plotted against *t*, the statistical thickness of the film (not shown). The fact that the initial region of the *t*-plot can be extrapolated to the origin confirms the absence of micropores at low p/p_0.

The adsorption isotherm for calcined CrMCM-41-(40) is also a type IV adsorption isotherm with H2 hysteresis in the range $0.35 < p/p_0 < 0.45$. At $p/p_0 > 0.8-1.0$, the type IV isotherm shows a H3 hysteresis loop (Figure 13). H3 hysteresis is associated with the formation of macropores that are larger than mesopores.[41]

The pore size distribution curve for CrMCM-41-(100) shows a very narrow pore size distribution with pore size 33.4 Å and high surface area of 1308 m^2/g based on the BJH formula using the adsorption branch of the N_2 adsorption isotherm (Table 3). The thickness of the pore walls calculated from the size of the unit cell by subtracting the pore size is 18 Å. Such thick pore walls account for the high structural stability and the absence of lattice contraction upon calcination. CrMCM-41-(40) has a narrow pore size distribution with a pore size of 31 Å and smaller surface area of 867 m^2/g. However, the H3 hysteresis shows that large macropores are also formed. The continuous decrease in the surface area with increasing Cr content is similar to Ga- or Al-containing MCM-41.[28,42]

Discussion

Molecular Structure of Cr in CrMCM-41. Cr oxides supported on inorganic oxides such as silica, alumina, and molecular sieves are catalysts for the polymerization of ethylene,

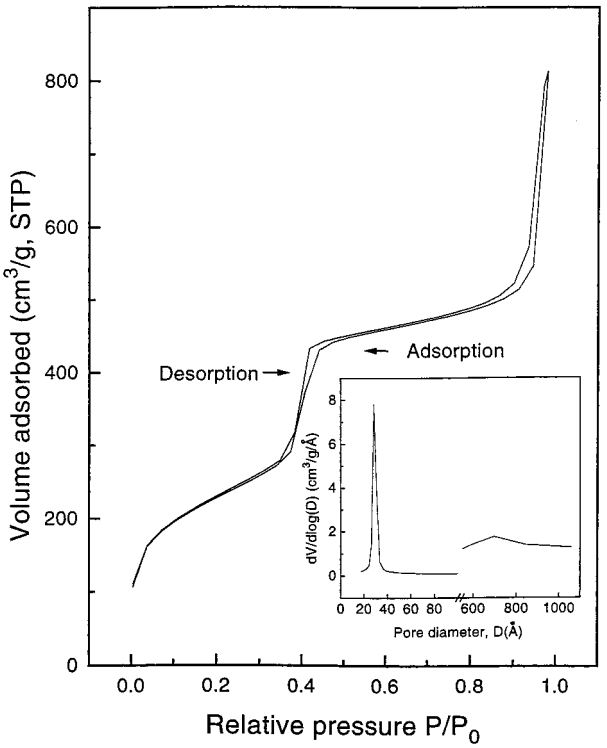

Figure 13. Adsorption−desorption isotherm of nitrogen at 77 K on calcined, dehydrated CrMCM-41-(40). The inset shows the BJH pore size distribution calculated from the adsorption branch of the isotherm.

TABLE 3: Pore Structure Parameters of CrMCM-41 Calculated from the Adsorption Branch of an N_2 Adsorption Isotherm Using The Barrett−Joyner−Halenda Formula

	surface area (A_{BJH} (m^2/g))	pore size (D_{BJH} (Å))	pore volume (cm^3/g)
CrMCM-41-(100)	1308	33.4	1.1
CrMCM-41-(80)	1063	33.6	0.9
CrMCM-41-(40)	867	31	1.2

hydrogenation−dehydrogenation, oxidation, and isomerization reactions.[1] The basis for the activity of Cr for such a wide spectrum of reactions lies in the variability of its oxidation states, coordination environments, and degrees of polymerization of Cr oxide species. The Philips Cr/silica polymerization catalyst is prepared by impregnating a chromium compound onto a wide pore silica and then calcining in oxygen to activate the catalyst.[15] This leaves Cr(VI) dispersed on the silica surface. The molecular structure of the anchored Cr(VI) has not been definitively determined and several molecular structures from monochromate to dichromate to polychromate have been proposed. Many researchers have measured a change in the hydroxyl population in these systems. A chromate species should react with two hydroxyls per chromium, whereas dichromate reacts with only one per chromium. However, the results from this approach are contradictory. Hogan[43] and McDaniel[44] concluded that CrO_3 attaches mainly as monochromate, while Zecchina et al.[45] and Krauss[46] reported that dichromate was the dominant species. Direct information about the molecular structure can be found by the application of diffuse reflectance spectroscopy and Raman spectroscopy. In as-synthesized CrMCM-41, the ESR intensity of Cr(III) increases while the line width of Cr(III) does not increase with Cr content. This indicates that the spin−spin interaction is weak and that Cr(III) is highly dispersed in as-synthesized CrMCM-41. In calcined CrMCM-41, UV−vis, FTIR, Raman, and ESR spectroscopies show that Cr(III) is oxidized to Cr(VI). A band around 440 nm characteristic of polychromate is absent in the UV−vis spectra and calcined CrMCM-41 has a Raman band at 986 cm^{-1} which indicates that Cr(VI) is present as a monochromate species.

The molecular structure of surface chromium oxide species is strongly dependent on the Cr loading, activation temperature, hydroxyl concentration, and surface area. Cr/SiO_2 with 2 wt % loading of Cr[37] and CrMCM-41-(40) have the same Cr loading and comparable BET surface areas of 735 m^2/g (Cr/SiO_2) and 867 m^2/g [CrMCM-41-(40)]. The number of SiOH groups/nm^2 for MCM-41 is between 2.5 and 3.0, which is less than that between 5 and 8/nm^2 on SiO_2.[38] So the Cr dispersion degree should be similar in Cr/SiO_2 and CrMCM-41. UV−vis and Raman spectroscopies clearly show that Cr in CrMCM-41 is similarly dispersed as in Cr/SiO_2.

The Cr ion is anchored on SiO_2 by an esterification reaction with the hydroxyl groups of silica. However, it is likely that some Cr(VI) is not produced by reaction of chromium ion with silanol groups. In such a case, $f_s = Q^3/Q^4$ should decrease with Cr content in calcined CrMCM-41. But, ^{29}Si MAS NMR shows that $f_s = Q^3/Q^4$ first increases and then decreases with Cr content in calcined CrMCM-41. There are two factors that may change f_s. If some Cr(III) ions are in the framework and during calcination are oxidized to Cr(VI), some Cr−O−Si bonds are broken, which produces $Si(OSi)_3OH$ (Q^3) and increases f_s with increasing chromium concentration in CrMCM-41. Second, silanol groups can interact with nonframework Cr during calcination to decrease f_s with increasing Cr in CrMCM-41 as occurs for Cr dispersed in SiO_2. These opposite factors can explain that f_s first increases and then decreases with increasing Cr if it is postulated that framework Cr predominates at low Cr concentration and nonframework Cr predominates at high Cr concentration. The Raman spectrum of CrMCM-41 also indicates that Cr possibly enters the second coordination sphere of framework silicons since we only observe a band at 986 cm^{-1} in the Raman spectrum of CrMCM-41-(40). N_2 adsorption shows macropores in CrMCM-41-(40) and that the surface area decreases significantly from 1308 m^2/g for CrMCM-41-(100) to 867 m^2/g for CrMCM-41-(40), possibly corresponding to partial structural collapse upon calcination. Therefore, we conclude that part of the Cr(III) is incorporated in the MCM-41 wall. After calcination, Cr(III) is oxidized to Cr(VI) and breaks Si−O−Cr bonds.

Calcination CrO_3/silica at low chromium loading retains Cr(VI), but at higher loading CrO_3 decomposes to Cr_2O_3 and O_2.[15] If this occurs for CrMCM-41-(40), Cr_2O_3 with Cr(III) should be observed in the UV−vis and ESR spectra. This is not observed so it appears that CrMCM-41-(40) corresponds to low loading.

Coordination and Reactivity of Cr in CrMCM-41. The chemistry of Cr(V) in molecular sieves is diverse and Cr(V) can have different coordination geometries as illustrated in Table 4. In ion-exchanged, oxidized Cr-mordenite, two different Cr(V) were reported; one is near the wall of a main channel with square pyramidal geometry and the other is at the junction between a main channel and a side pocket with distorted tetrahedral geometry.[47] Another interpretation was that the tetrahedral coordination of Cr(V) may be due to the replacement of Si(IV) by Cr(V) in the oxygen tetrahedron of the mordenite framework.[10b] For hydrothermally synthesized alumina-free CrZSM-5, after oxidative calcination most chromium ions aggregate into α-Cr_2O_3 microcrystals on the external surface of ZSM-5. However, some chromium remains stabilized in the zeolite structure as Cr(V) ions in two sites. The site with $g_\perp = 1.986$ and $g_\parallel = 1.913$ was assigned to Cr(V) with distorted tetrahadral

TABLE 4: ESR Signals of Cr(V) in Chromium-Containing Molecular Sieves and Their Assignments

chromium-containing molecular sieves	treatment	ESR signal	assignment	refs
ion-exchanged Cr-mordenite	oxidized	$g_{xx} = 1.9867$; $g_{yy} = 1.9720$; $g_{zz} = 1.9110$	square-pyramidal Cr(V) ion in a main channel	46
		$g_\perp = 1.9947$; $g_\parallel = 1.9070$	distorted tetrahedral Cr(V) at a junction between a main channel and a side pocket	
ion-exchanged Cr-ZSM-5	calcined	$g_\perp = 1.986$; $g_\parallel = 1.913$	distorted tetrahedral Cr(V) inside ZSM-5 channels	47
		$g_\perp = 1.796$; $g_\parallel = 1.960$	Cr(V) in ZSM-5 framework	
impregnated Cr/SiO_2	calcined	$g_1 = 1.845$; $g_2 = 1.968$; $g_3 = 1.975$	tetrahedral Cr(V)	48
synthesized CrAlMCM-41	calcined	$g_\perp = 1.974$; $g_\parallel = 1.950$	Cr(V) species	49
		$g_\perp = 1.982$; $g_\parallel = 1.947$		
synthesized CrMCM-41	calcined evacuated	$g_\perp = 1.966$; $g_\parallel = 1.868$	tetrahedral Cr(V)	this work

geometry located inside ZSM-5 channels. The other site with $g_\perp = 1.976$ and $g_\parallel = 1.960$ was assigned to distorted five-coordinated Cr(V) in recessed positions from the main channel.[48] Cr(V) species with tetrahedral geometry with $g_1 = 1.895$, $g_2 = 1.968$, and $g_3 = 1.975$ are formed in 0.44 wt % CrO_3 impregnated on SiO_2 and heated in O_2 at 773 K, followed by evacuation at 393 K.[49] When AlMCM-41 and CrO_3 are mixed, ground, and then heated at 500 °C, two axial Cr(V) species ($g_\perp = 1.974$ and $g_\parallel = 1.950$; $g_\perp = 1.982$ and $g_\parallel = 1.947$) were observed.[50] The parameters of these two species are very similar and may indicate a distribution of g values around a mean value rather than two distinct sites.

The absence of Al modulation in two-pulse ESEM spectra of Cr grafted AlMCM-41 suggested that the sites to which Cr is grafted did not have ^{27}Al in their immediate environment.[50] Based on ESR of Cr(V) interaction with O_2, we conclude that $Cr(VI)-O_2^-$ in calcined CrMCM-41 is produced as follows. During calcination of CrMCM-41, Cr(III) is oxidized to tetrahedral Cr(V), which then coordinates with one molecule of O_2 to form a five-coordinated square-pyramidal $Cr(V)-O_2$ complex. At elevated temperature, electron transfer occurs between Cr(V) and O_2 to form $Cr(VI)-O_2^-$. After evacuation at elevated temperature, an electron transfers back to Cr(VI) to release O_2 and form tetrahedral Cr(V).

While the structure of Cr(V) on various zeolites and supports has received much attention, its coordination and reactivity with polar and nonpolar molecules have been less studied. The coordination change for Cr(V) in SiO_2, Al_2O_3, ZrO_2, TiO_2, and SnO_2 upon adsorption of NH_3 and H_2O has been investigated by ESR.[49] And Cr(V) interaction with various adsorbates in ZSM-5,[48] mordenite,[47] SAPO-5,[11] and SAPO-11[13] has been investigated by ESR and ESEM. ND_3 interaction with Cr(V)-grafted AlMCM-41 was also studied.[50]

When ND_3 is adsorbed on dehydrated CrMCM-41, two new Cr(V) species with axially symmetric ESR parameters ($g_\perp^N = 1.989$ and $g_\parallel^N = 1.967$ for species N and $g_\perp^O = 1.989$ and $g_\parallel^O = 1.932$ for species O) are observed. After this sample is sealed and kept at room temperature for several days, species O remains and species N disappears. The larger $g_\parallel$ values for Cr(V) species N versus that for species O suggests that species N has a stronger interaction with Cr(V) than does species O. This follows since $g_\parallel = g_e - 8\lambda/\Delta$ where λ is the spin−orbit coupling constant with Δ the transition energy that describes the magnitude of the interaction between Cr(V) and ND_3. So we assume that Cr(V) occurs at two different sites, on the wall surfaces of MCM-41 and inside these walls. Cr(V) on the wall surfaces can easily interact with NH_3 while Cr(V) inside the wall has a weaker interaction with NH_3. Similar cases were found for Cr(V) in ZSM-5 and SAPO-11.[48,13] Adsorption of NH_3 on CrZSM-5 results in full replacement of Cr(V) located inside ZSM-5 channels by a new species, while a second Cr(V) species inside the ZSM-5 framework remains intact.[48] No change was seen for NH_3 adsorption on CrAPSO-11 for 0.5 h while solid-state ion-exchanged (S)Cr−SAPO-11 reacts rapidly with NH_3.[13] Analysis of the three-pulse ESEM spectra of CrMCM-41 with adsorbed ND_3 to form only species O indicates that Cr(V) coordinates two ND_3 molecules. This result is similar to two NH_3 molecules interacting with Cr(V) supported on SiO_2, as shown by the superhyperfine splitting in $g_\perp$ by interaction with $^{15}NH_3$.[47]

The interaction of Cr(V) with C_2H_4 has not been studied before, although Cr(II) interaction with C_2H_4 was studied by IR since this interaction is postulated as the active state for the polymerization of ethylene by the Philips chromium catalyst.[51] ESR and ESEM of CrMCM-41 interaction with C_2H_4 show that a part of Cr(V) directly coordinates with one molecule of ethylene to form a five-coordinate complex $Cr^V(C_2D_4)$. A similar result was found for adsorption of C_2H_4 onto liquid-state ion-exchanged, oxidized Cr-SAPO-5.[11] Species I indicates that Cr(V) is possibly reduced to Cr(IV) during further contact. A similar case was observed for the Philips catalyst.[52] Contact of ethylene with surface Cr results in Cr(IV) compounds.[52] Further reduction results in the formation of Cr(III) as shown by a broad ESR spectrum.

The interaction of Cr(V) with CD_3OH in CrMCM-41 shows that two species K and L are formed. Species K is more stable than species L. Both species are reduced to Cr(II) during continued exposure to methanol. ESEM shows that Cr(V) interacts with one molecule of CD_3OH to form species K, which is similar to Mo(V) supported on SiO_2 interacting with one molecule of CD_3OH.[53] The number of methanols coordinating with a transition metal depends on the transition metal ions and the zeolite structure. Cu(II) in liquid state ion-exchanged Cu(II)-AlMCM-41 directly coordinates two molecules of methanol.[54] The ESEM data for solid ion-exchanged Cr-SAPO-11 with adsorbed CD_3OH also indicate coordination to two methanols. This is also supported by a nearly isotropic ESR signal, which shows that tetrahedral Cr(V) coordinates two water methanol molecules to form an octahedral $Cr^V(CD_3OH)_2$ complex.[13]

Conclusions

A series of mesoporous chromium-containing CrMCM-41 molecular sieves (CrMCM-41) with variable Si/Cr ratios have been synthesized and characterized by physicochemical methods. XRD, EPMA, UV−vis, and ESR show that as-synthesized CrMCM-41 has the MCM-41 structure and contains only atomically dispersed Cr(III). FTIR, UV−vis, and Raman reveal that Cr(VI) monochromate exists in calcined CrMCM-41. ^{29}Si MAS NMR and N_2 adsorption show that part of the chromium is incorporated into the MCM-41 structure. ESR shows that $Cr(VI)-O_2^-$ exists in calcined CrMCM-41 and transforms to Cr(V) after evacuation above 150 °C. The interaction of Cr(V)

with O_2, CO, C_2H_4, ND_3, CD_3OH, and D_2O shows that Cr(V) occurs at two different sites. One site is more accessible to these adsorbates.

Acknowledgment. This research was supported by the National Science Foundation, the Robert A. Welch Foundation, and the University of Houston Energy Laboratory. We thank Dr. M. Narayana for the NMR and Dr. R. Czernuszewicz for the Raman measurements.

References and Notes

(1) Weckhuysen, B. M.; Wachs I. E.; Schoonheydt, R. A. *Chem. Rev.* **1996**, 96, 3327.
(2) Muzart, J. *Chem. Rev.* **1992**, 92, 113.
(3) Flanigen, E. M.; Lok, B. M.; Patton, R. L.; Wilson, S. T. U.S. Patent 4,738,887, 1988.
(4) Wan, B.; Huang, K.; Yang, T.; Tai, C. *J. Chin. I. Ch. E.* **1991**, *22*, 17.
(5) (a) Chen, J.; Dakka, J.; Sheldon, R. *Appl. Catal. A* **1994**, *108*, L1. (b) Chen, J.; Haanepen, M.; van Hooff, J.; Sheldon, R. In *Zeolites and Related Microporous Materials: State of the Art;* Weitkamp, J., Karge, H. G.; Pfeifer, H., Holderich, W., Eds.; Elsevier: Amsterdam, 1994; p 973 [*Stud. Surf. Sci. Catal.* **1994**, *84*, 973]. (c) Chen, J.; Sheldon, R. *J. Catal.* **1995**, *153*, 1. (d) Chen, J. D.; Lempers, E. B.; Sheldon, R. *J. Chem. Soc., Faraday Trans.* **1996**, *92*, 1807.
(6) Escalante, D.; Giraldo, L.; Pinto, M.; Pfaff, C.; Sazo, V.; Matjushin, M.; Mendez, B.; Lopez, C.; Machado, F.; Goldwasser, J.; Ramirez De Agudelo, M. *J. Catal.* **1997**, *169*, 176.
(7) Chapus, T.; Tuel, A.; Taarit, Y.; Naccache, C. *Zeolites* **1994**, *14*, 349.
(8) Nakamura, O.; Mambrim, J.; Pastore, H.; Vichi, E.; Gandra, F.; Silva, E.; Vargas, H.; Pelzl, J. *J. Chem. Soc., Faraday Trans.* **1992**, *88*, 2071.
(9) Yuvaraj, S.; Palanichamy, M.; Krishnasamy, V. *Chem. Commun.* **1996**, 2707.
(10) (a) Weckhuysen, B. M.; Schoonheydt, R. A. *Zeolites* **1994**, *14*, 360. (b) Weckhuysen, B. M.; Schoonheydt, R. A.; Mabbs, F. E.; Collison, D. *J. Chem. Soc., Faraday Trans.* **1996**, *92*, 2431.
(11) Zhu, Z.; Kevan, L. *Phys. Chem. Chem. Phys.* **1999**, *1*, 199.
(12) Giraldo, L.; Pfaff, C.; Lopez, C.; Machado, F.; Mendez, B.; Goldwasser, J.; Ramirez De Agudelo, M.; Rondon, S.; Houalla, M.; Hercules, D. *Surf. Interface Anal.* **1996**, *24*, 863.
(13) Zhu, Z.; Wasowicz, T.; Kevan, L. *J. Phys. Chem. B* **1997**, *101*, 10763.
(14) Rajic, N.; Stojakovic, D.; Hocevar, S.; Kaucic, V. *Zeolites* **1993**, *13*, 384.
(15) (a) McDaniel, M. *Adv. Catal.* **1985**, *33*, 47. (b) McDaniel, M. *Ind. Eng. Chem. Res.* **1988**, *27*, 1559.
(16) Weckhuysen, B. M.; Bensalem, A.; Schoonheydt, R. A. *J. Chem. Soc., Faraday Trans.* **1998**, *94*, 2011.
(17) Kresge, C. T.; Leonowicz, M. E.; Roth, W. J.; Vartuli, J. C.; Beck, J. S. *Nature* **1992**, *359*, 710.
(18) Beck, J. S.; Vartuli, J. C.; Roth, W. J.; Leonowicz, M. E.; Kresge, C. T.; Schmitt, K. D.; Chu, C. T.-W.; Olson, D. H.; Sheppard, E. W.; McCullen, S. B.; Higgins, J. B.; Schlenker, J. L. *J. Am. Chem. Soc.* **1992**, *114*, 10834.
(19) Zhao, D.; Feng, J.; Huo, Q.; Melosh, N.; Fredrickson, G.; Chmelka, B.; Stucky, G. D. *Science* **1998**, *279*, 548.
(20) Zhao, D.; Huo, Q.; Feng, J.; Chmelka, B.; Stucky, G. D. *J. Am. Chem. Soc.* **1998**, *120*, 6024.
(21) Ulagappan, N.; Rao, C. N. R. *Chem. Commun.* **1996**, 1047.
(22) Zhang, W.; Pinnavaia, T. J. *Catal. Lett.* **1996**, 38, 261.
(23) Kevan, L. In *Time Domain Electron Spin Resonance;* Kevan, L., Schwartz, R. N., Eds.; Wiley: New York, 1979; Chapter 8.
(24) Dikanov, S. A.; Tsvetkov, Yu. D. *Electron Spin-Echo Envelope Modulation Spectroscopy*; CRC: Boca Raton, FL, 1992.
(25) Barrett, E. P.; Joyner, L. G.; Halenda, P. P. *J. Am. Chem. Soc.* **1951**, *73*, 373.
(26) Corma, A.; Kan, Q.; Rey, F. *Chem. Commun.* **1998**, 579.
(27) Cheng, C.; Park, D.; Klinowski, J. *J. Chem. Soc., Faraday Trans.* **1997**, *93*, 193.
(28) Cheng, C.; He, H.; Zhou, W.; Klinowski, J.; Goncalves, J.; Gladden, L. *J. Phys. Chem.* **1996**, *100*, 390.
(29) McCarthy, P.; Lauffenburger, J.; Skonezny, P.; Rohrer, D. *Inorg. Chem.* **1981**, *20*, 1566.
(30) Vuurman, M. A.; Wachs, I. E.; Stufkens, D. J.; Oskam, A. *J. Mol. Catal.* **1993**, *80*, 209.
(31) Schwarz, S.; Corbin, D. R.; Vega, A. J. In *Materials Research Society Symposium Proceedings*; Lobo, R. F., Beck, J. S., Suib, S. L., Corbin, D. R., Davis, M. E., Iton, L. E., Zones, S. I., Eds.; Materials Research Society: Pittsburgh, PA, 1996; Vol. 431, p 137.
(32) Mambrim, J.; Pastore, H.; Davano, C.; Vichi, E.; Nakamura, O.; Vargas, H. *Chem. Mater.* **1993**, *5*, 166.
(33) Giannetto, G.; Papa, L.; Yanez, F.; Goldwasser, M.; Linares, C.; Moronta, D.; Mendez, B.; Navarro, C.; Monque, R. *Zeolites* **1997**, *19*, 169.
(34) Luan, Z.; Xu, J.; He, H.; Klinowski, J.; Kevan, L. *J. Phys. Chem.* **1996**, *100*, 19595.
(35) Luan, Z.; Meloni, P.; Czernuszewicz, R.; Kevan, L. *J. Phys. Chem.* **1997**, *101*, 9046.
(36) Vuurman, M.; Wachs, I. E. *J. Phys. Chem.* **1992**, *96*, 5008.
(37) Weckhuysen, B. M.; Wachs, I. E. *J. Phys. Chem.* **1996**, *100*, 14437.
(38) Zhao, X. S.; Lu, G. Q.; Whittaker, A. K.; Millar, G. J.; Zhu, H. Y. *J. Phys. Chem.* **1997**, *101*, 6525.
(39) Alba, M. D.; Luan, Z.; Klinowski, J. *J. Phys. Chem.* **1996**, *100*, 2178.
(40) Dyrek, K.; Che, M. *Chem. Rev.* **1997**, *97*, 305.
(41) Sing, K. S. W.; Everett, D. H.; Haul, R. A. W.; Moscou, L.; Pierotti, R. A.; Rouquerol, J.; Siemieniewska, T. *Pure Appl. Chem.* **1985**, *57*, 603.
(42) Luan, Z.; He, H.; Zhou, W.; Cheng, C.; Klinowski, J. *J. Chem. Soc., Faraday Trans.* **1995**, *91*, 2955.
(43) Hogan, J. P. *J. Polym. Sci.* **1970**, *8*, 2637.
(44) McDaniel, M. P. *J. Catal.* **1982**, *76*, 37.
(45) Zecchina, A.; Garrone, E.; Ghiotti, G.; Morterra, C.; Borello, E. *J. Phys. Chem.* **1975**, *79*, 966.
(46) Krauss, H. L.; Stach, H. Z. *Anorg. Allg. Chem.* **1975**, *414*, 97.
(47) Huang, M.; Deng, Z.; Wang, Q. *Zeolites* **1990**, *10*, 272.
(48) Kucherov, A. V.; Slinkin, A. A.; Beyer, G. K.; Borbely, G. *Zeolites* **1995**, *15*, 431.
(49) Cordishi, D.; Campa, M. C.; Indovina, V.; Occhiuzzi, M. *J. Chem. Soc., Faraday Trans.* **1994**, *90*, 207.
(50) Luca, V.; MacLachlan, D. J.; Bramley, R.; Morgan, K. *J. Phys. Chem.* **1996**, *100*, 1793.
(51) Bade, O. M.; Blom, R.; Dahl, I. M.; Karlsson, A. *J. Catal.* **1998**, *173*, 460.
(52) Krauss, H. L. *J. Mol. Catal.* **1989**, *46*, 97.
(53) Narayana, M.; Zhan, R. Y.; Kevan, L. *J. Phys. Chem.* **1985**, *89*, 636.
(54) Poppl, A.; Hartmann, M.; Kevan, L. *J. Phys. Chem.* **1995**, *99*, 17251.